Anionic Species Determination in $CaSiO_3$ Glass Using Two-Dimensional ^{29}Si NMR

Ping Zhang and Philip J. Grandinetti*,†

Department of Chemistry, The Ohio State University, 120 W. 18th Avenue, Columbus, Ohio 43210-1173

Jonathan F. Stebbins‡

Department of Geological and Environmental Sciences, Stanford University, Stanford, California 94305-2115

Received: December 18, 1996; In Final Form: March 17, 1997⊗

The structure of the alkaline earth silicate glass $CaSiO_3$ has been investigated using a two-dimensional ^{29}Si NMR experiment that correlates the isotropic magic-angle-spinning (MAS) spectrum with an anisotropic off-magic-angle-spinning spectrum. Although the one-dimensional magic-angle-spinning (MAS) spectrum is completely unresolved, all five types of SiO_4 tetrahedra (represented by the notation $Q^{(n)}$, where $n = 0$-4 representing the number of bridging oxygen) can be resolved and quantified on the basis of the separated anisotropic line shapes in the 2D spectrum. The distribution of isotropic chemical shifts derived from the 2D spectrum suggests that in the case of $CaSiO_3$ glass the conventional approach of fitting the one-dimensional MAS spectrum with overlapping Gaussian line shapes would lead to significant errors in $Q^{(n)}$ quantification. The equilibrium constants for the disproportionation reaction $2Q^{(n)} \rightleftharpoons Q^{(n-1)} + Q^{(n+1)}$ with $n = 1$, 2, and 3 were determined from the 2D spectrum to be 0.105 ± 0.019, 0.156 ± 0.005, and 0.106 ± 0.022, respectively. These results clearly indicate a significantly greater deviation from a binary model of $Q^{(n)}$ species disproportionation in alkaline earth silicate melts when compared to alkali silicate melts and thus suggest a relatively more disordered structure.

Introduction

Measurements of the relative abundances of anionic species in silicate glasses are essential for any structure-based model of thermodynamic or transport properties of silicate liquids and magmas. Probably the most fundamental aspect of this speciation is the distribution of silicate tetrahedra with varying numbers (n) of bridging oxygens, commonly described as $Q^{(n)}$ species. A large number of papers have shown that such populations can be estimated from peak intensities in Raman spectra[1−5] and, more recently, from ^{29}Si nuclear magnetic resonance (NMR) spectra.[6−8] Recognizing the inherently quantitative nature of the latter technique, NMR data for alkaline earth silicate glasses have been used to calibrate Raman absorption cross sections, improving the accuracy of fits of spectra over a wide range of composition and temperature.[3,5]

Unfortunately, even for alkali silicates, ^{29}Si magic-angle-spinning (MAS) NMR spectra are incompletely resolved, often necessitating the use of curve fitting to extract peak intensities. Gaussian peak shapes are usually assumed because they allow good fits, are simple to calculate, and perhaps have some justification in terms of a random distributions of parameters and the central limit theorem; in general, however, a Gaussian distribution of structural features, such as interatomic distances, and bond angles, will not necessarily map into a Gaussian distribution of NMR peak positions. In the special case of the $Q^{(4)}$ species, static spectra can give accurate abundances without curve fitting (this species has a uniquely narrow peak), but this approach is applicable over only a relatively narrow range of compositions.[9,10] The situation is worse for binary alkaline earth silicates: in this case the ^{29}Si MAS spectra are usually unresolved, presumably because of greater disorder.[6,11] NMR spectroscopists have generally avoided analyzing such data by unconstrained curve fitting because of the large uncertainties involved and doubts about the validity of Gaussian peak components.[12] However, a published ^{29}Si spectrum for $CaSiO_3$ glass has recently been digitized and fitted with Gaussians to yield $Q^{(1)}$, $Q^{(2)}$, and $Q^{(3)}$ concentrations,[4,13] which were then used to calibrate Raman peak intensities and to model a large number of alkaline earth glass and liquid spectra. We have recently reported on a two-dimensional NMR technique that gives much improved determinations of $Q^{(n)}$ species concentration without the necessity of fitting with Gaussian peaks, and we have demonstrated its accuracy and precision in a well-understood sodium silicate binary composition.[14] In this paper we show the first application of this approach to a glass with a completely unresolved ^{29}Si MAS spectrum ($CaSiO_3$). In this example, robust $Q^{(n)}$ species abundances can again be derived, and the presence of even low-abundance species can be confirmed.

Experimental Section

Nuclear Magnetic Resonance Spectroscopy. As illustrated in Figure 1, $Q^{(n)}$ species exhibit anisotropic NMR line shapes under static or off-magic angle spinning conditions due to the anisotropy (CSA) of the chemical shift interaction. The line shape anisotropy[17] is characterized by two main parameters: axiality, Δ, and asymmetry parameter, η. The width of the anisotropy is determined primarily by the magnitude of $\triangle$, and the line shape by η. $Q^{(0)}$ and $Q^{(4)}$ sites have the smallest axiality due to their highly symmetric environment. $Q^{(1)}$ and $Q^{(3)}$ sites have relatively large axialities that are opposite in sign and have low asymmetry parameters, which reflect the axial symmetry of their environments. $Q^{(2)}$ sites also have relatively large axialities; however, because of their divergence from axial symmetry, they have an intermediate asymmetry parameter.

Under MAS conditions, where anisotropic broadening (i.e., information on Δ and η) is removed, the five $Q^{(n)}$ species are

* Author to whom correspondence should be addressed.
† FAX: (614) 292-1685. E-mail: grandinetti.1@osu.edu.
‡ FAX: (415) 725-2199. E-mail: stebbins@pangea.stanford.edu.
⊗ Abstract published in *Advance ACS Abstracts,* May 1, 1997.

S1089-5647(97)00034-5 CCC: $14.00

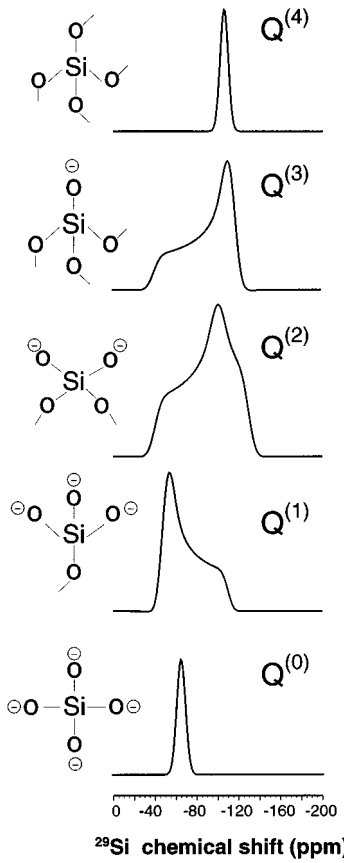

Figure 1. One-dimensional ^{29}Si off-magic-angle-spinning (i.e., 90°) NMR line shapes for the five different silicate tetrahedral environments in silicate glasses. Line shape parameters are based on typical values found in crystalline compounds.[15,16]

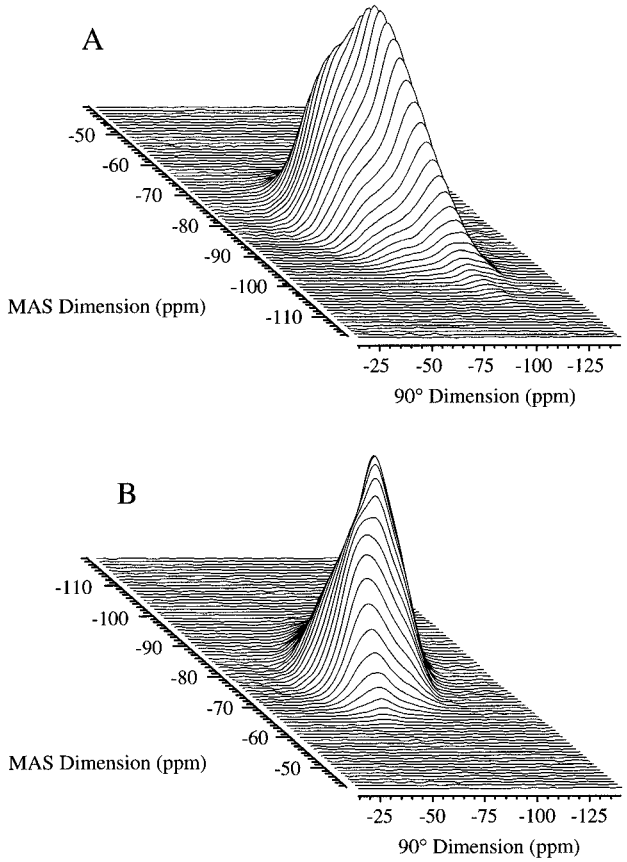

Figure 2. Stack plots of the two-dimensional ^{29}Si (MAS, 90°) correlation spectrum. In A the spectrum is plotted with the most negative chemical shifts in the MAS dimension in the front. In B the spectrum is plotted with the least negative chemical shifts in the front.

identified mainly by their isotropic position, δ_{iso}, which approximately ranges from −70 ppm for $Q^{(0)}$ to −110 ppm for $Q^{(4)}$.[18] I n crystalline silicates the isotropic line widths are usually on the order of 1 ppm or less, and it is often possible to resolve not only different $Q^{(n)}$ species but also crystallographically distinct $Q^{(n)}$ species of the same type (i.e., same n). In contrast, in a glass the isotropic line widths are inhomogeneously broadened to over 10 ppm due to a continuous distribution of isotropic chemical shifts, which arise from a continuous structural distribution in local structure (e.g., Si−O−Si angles, nonbridging oxygen−alkali distances, and higher coordination sphere structures). This broadening results in considerable overlap of $Q^{(n)}$ resonances and thus significant uncertainties when attempting to quantify the relative $Q^{(n)}$ populations from isotropic MAS line shapes. As we have shown previously,[14] the separation of anisotropic line shapes obtained in a two-dimensional NMR spectrum correlating isotropic and anisotropic line shapes provides a means of determining the distributions of $Q^{(n)}$ species without any *a priori* assumptions about the distribution and also significantly reduces the covariances between best fit parameters, thus increasing the precision in quantifying site populations.

We have used a slightly modified version of the magic-angle-flipping NMR experiment by Bax et al.[19] where the NMR spectrum while spinning at the magic angle is correlated with that while spinning at an axis perpendicular to the magnetic field. When spinning perpendicular to the magnetic field, the static sample anisotropic line shapes are scaled[20] by a factor of −0.5, as shown in Figure 1. Our sequence differs from the original experiment of Bax et al.[19] by the addition of an additional π pulse before t_2 to improve sensitivity and to give pure absorption mode line shapes.[21] The experiment was performed on a Chemagnetics 9.4 (79.48 MHz for ^{29}Si) NMR spectrometer using a modified version of a home-built DAS probe described earlier.[21] The experiment was done at ambient temperature with a sample spinning rate of 10.4 kHz. The ^{29}Si relaxation time was measured using a saturation recovery experiment under MAS conditions, and T_1 values were found to be 50.3 s. A pulse delay of 300 s was chosen. No changes in peak shape as a function of delay time were observed, indicating no differential relaxation among different species. The angle pair (90° and 54.74°) was employed with detection made at 54.74°. $\pi/2$ times were chosen to be 4.4 μs at 54.74° and 5.7 μs at 90°. The number of scans was 32; the number of $t_1 \times t_2$ points is 61 × 256, with a dwell time of 25 μs and 25 μs, respectively.

Sample Preparation and Characterization. The sample was synthesized from high-purity $CaCO_3$ and 95% ^{29}Si-enriched SiO_2 (Oak Ridge Laboratory), with 0.1 wt % CoO added to enhance spin−lattice relaxation. The starting material was decarbonated at 900 °C and then melted for 2 h at about 1600 °C. The weight loss during synthesis was within 0.1% of nominal, indicating close to ideal stoichiometry. High-precision electron microprobe analyses on multiple grains of the glass, accounting for the isotopic enrichment, gave a molar Ca/Si ratio of 0.99 ± 0.01.

Results

Stack plots of the ^{29}Si two-dimensional (90°, MAS) correlation NMR spectrum of $CaSiO_3$ glass are shown in Figure 2. In Figure 2A the spectrum is plotted with the most negative isotropic chemical shifts in the MAS dimension to the front. Recalling the characteristic anisotropic line shapes shown in

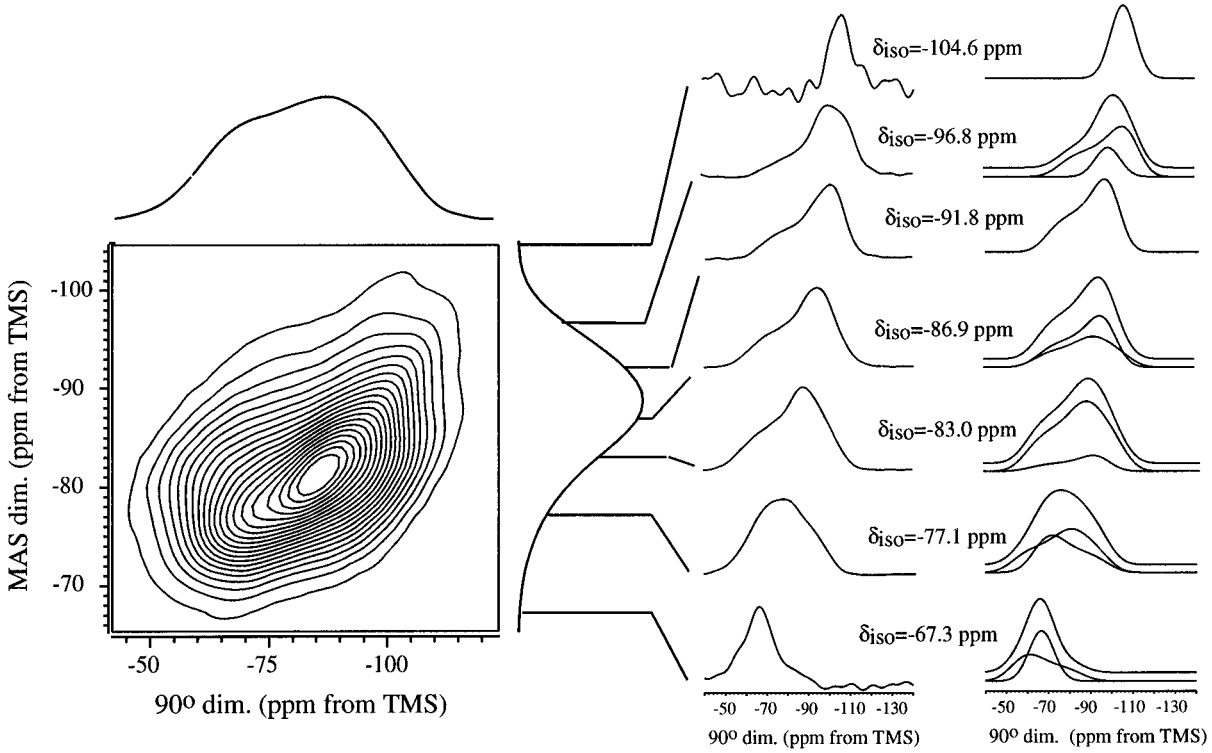

Figure 3. Contour plot with projection on each dimension. Twenty equally spaced contour lines are drawn at levels ranging from 3 to 93% of the maximum intensity in the spectrum. On the right are selected cross sections and their "best-fit" curves. Forty-five cross sections from $\delta_{iso} = -65.31$ ppm to -108.56 ppm were analyzed. The average χ^2_ν value was 48.47, with a standard deviation of 75.32.

Figure 1, it is clear from the 90° dimension that in the region of −110 ppm a low-intensity symmetric line shape attributed to $Q^{(4)}$ species can be observed. Moving to less negative chemical shifts in the −100 ppm region, anisotropic chemical shift line shapes characteristic of negative axiality and nearly zero asymmetry parameters are observed and are attributed to $Q^{(3)}$ species. In the region of −85 ppm the anisotropic line shapes are dominated by anisotropic chemical shift, and line shapes with $\eta = 0.70$ are attributed to $Q^{(2)}$ species. In Figure 2B the same spectrum is plotted with the least negative isotropic chemical shifts in the MAS dimension to the front. In the region of −65 ppm a very weak symmetric line shape attributed to $Q^{(0)}$ species is observed. Moving to more negative chemical shifts in the −75 ppm region, anisotropic chemical shift line shapes characteristic of positive axiality are observed and are attributed to $Q^{(1)}$.

The anisotropic line shapes in the individual cross sections taken parallel to the 90° dimension were least-squares analyzed to obtain the relative contribution of each $Q^{(n)}$ species to the MAS intensity at the MAS frequency correlated to that cross section. A contour plot along with representative cross sections and best-fit simulations is also shown in Figure 3. Again, this approach has the advantage that the parameter uncertainties in each cross section are completely uncorrelated with parameter uncertainties in other cross sections. The chemical shift anisotropy line shape for each site was modeled using five parameters. These were (1) an isotropic chemical shift position δ_{iso}, (2) a chemical shift tensor axiality Δ, (3) a chemical shift tensor asymmetry parameter η, (4) an integrated intensity, and (5) a Gaussian smoothing function. All sites in each cross section shared the same isotropic frequency and that value was fixed by the isotropic dimension. In least-squares analyses those cross sections dominated by one $Q^{(n)}$ species showed little variations in Δ, η, and Gaussian line broadening for the line shape of the dominant species. Therefore, in the final least-squares analysis of each cross section the chemical shift tensor

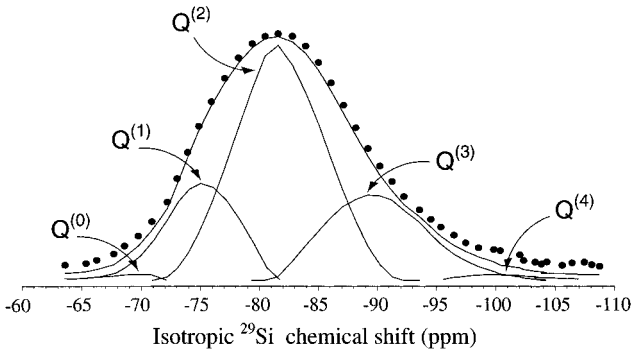

Figure 4. Separated isotropic line shapes for each $Q^{(n)}$. The reconstructed ^{29}Si MAS spectrum of $CaSiO_3$ glass from the sum of the five isotropic line shapes is shown above, along with the observed MAS spectrum shown in black dots.

axiality Δ and asymmetry parameter η for a given $Q^{(n)}$ site were held fixed at the values obtained when that $Q^{(n)}$ site was the dominate species in the cross section. All sites were constrained to have the same Gaussian smoothing function equivalent to 1100 Hz, and Δ and η were fixed at $\Delta = 40.0$ ppm, $\eta = 0.4$ for $Q^{(1)}$, $\Delta = -48.3$ ppm, $\eta = 0.7$ for $Q^{(2)}$, $\Delta = -45.4$ ppm, $\eta = 0.01$ for $Q^{(3)}$, and $\Delta = 0.0$ ppm, $\eta = 0.0$ for $Q^{(4)}$ and $Q^{(0)}$. All parameters are in general agreement with crystalline silicate results.[15,16]

Discussion

The MAS spectrum obtained from the projection of the two-dimensional spectrum onto the MAS dimension is shown in Figure 4 along with the individual component line shapes for each of the $Q^{(n)}$ species present in the glass. The component line shapes were constructed from the integrated intensities obtained from the least-squares analyses of the anisotropic cross sections. To quantify deviations from a Gaussian shape for each of the $Q^{(n)}$ component line shapes, we have calculated the mean

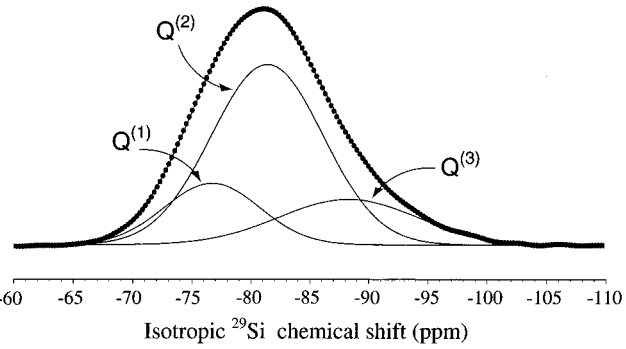

Figure 5. Deconvoluted Gaussian line shapes for each $Q^{(n)}$ obtained from a least-squares analysis of the one-dimensional ^{29}Si MAS spectrum of $CaSiO_3$ glass. The observed MAS spectrum is shown in black dots.

TABLE 1: Relative Area, Mean Position, Variance, Skewness, and Kurtosis for Each $Q^{(n)}$ Component Line Shape Constructed from the Integrated Intensities Obtained from the Least-Squares Analyses of the Two-Dimensional ^{29}Si NMR Anisotropic Cross Sections[a]

	relative area	mean position	variance	skewness	kurtosis
$Q^{(0)}$	0.72 ± 0.13%				
$Q^{(1)}$	19.33 ± 0.28%	−74.6	8.0	0.31	0.08
$Q^{(2)}$	54.68 ± 0.34%	−81.7	13.8	0.01	−0.47
$Q^{(3)}$	24.14 ± 0.53%	−90.4	16.9	−0.40	−0.16
$Q^{(4)}$	1.13 ± 0.01%				

TABLE 2: Relative Area, Mean Position, and Variance for Each $Q^{(n)}$ Component Gaussian Line Shape Obtained in the Least-Squares Analyses of the One-Dimensional ^{29}Si MAS NMR Spectrum of $CaSiO_3$ Glass.[a]

	relative area	mean position	variance
$Q^{(1)}$	18 ± 3%	−76.9	16.3
$Q^{(2)}$	63 ± 4%	−81.5	22.5
$Q^{(3)}$	19 ± 4%	−88.4	34.6

[a] Confidence limits are quoted as ± one unit of standard deviation.

position, variance, skewness, and kurtosis for each $Q^{(n)}$ line shape. These are given in Table 1. The skewness and kurtosis are nearly zero in all three cases, an indication that the assumption of Gaussian distributions is probably reasonable.

A simplifying assumption in our analysis of the 2D spectrum is that there is overlap of no more than two different $Q^{(n)}$ species at a given isotropic frequency. With the exception of the low-intensity $Q^{(0)}$, we believe this assumption is valid on the basis of the tabulated ranges of $Q^{(n)}$ isotropic chemical shifts in crystalline silicates.[15,16] Indeed, we believe this is also a strong criticism of the fit of the 1D MAS spectrum of $CaSiO_3$ glass using Gaussian line shapes as shown in Figure 5 and in the variances in Table 2. The least-squares analysis of the 1D MAS spectrum contains a $Q^{(3)}$ component line shape that unrealistically spans a chemical shift range that is almost twice that seen in crystalline silicates. The presence of $Q^{(3)}$ anisotropic cross sections at such extreme isotropic chemical shifts is not supported by our two-dimensional data. Clearly, a fit of the one-dimensional MAS spectrum alone to Gaussian line shapes for the $Q^{(n)}$ components would lead to significant errors in $Q^{(n)}$ quantification.

The relative populations for each of the five $Q^{(n)}$ species given in Table 1 should agree with the expected Ca/Si ratio of the charge balance equation

$$2[Q^{(0)}] + 1.5[Q^{(1)}] + 1[Q^{(2)}] + 0.5[Q^{(3)}] + 0[Q^{(4)}] = \text{Ca/Si} \quad (1)$$

Each $Q^{(n)}$ species has a charge of $-(4-n)$, which is balanced by the +2 charge of the calcium cation. The Ca/Si ratio calculated with eq 1 and the observed relative populations is 0.972 ± 0.006. This value agrees reasonably well with the analyzed composition and offers additional evidence for the accuracy of our new spectroscopic determination of the glass structure. The most likely explanation of the slight discrepancy in Ca/Si is the presence of oxide ions (O^{2-}) not bound to any Si, which are not accounted for in eq 1. If it is assumed that the actual Ca/Si ratio is 1.00, then the mole fraction of oxygen present as O^{2-} would be about 0.01. This value is not unreasonable given oxide ion activities determined at lower SiO_2 contents in $MO-SiO_2$ liquids (M = Ca, Fe, Ni, etc.) by thermochemical means,[22−24] although it is difficult to extrapolate such data down in temperature from the liquidus to the glass transition. It is also worth noting that several calcium silicates (e.g., Ca_3SiO_5) contain OCa_n groups, i.e., oxygen not bound to silicon.

TABLE 3: Comparison of Equilibrium Constants[a] for the Disproportionation Reaction $2Q^{(n)} \rightleftharpoons Q^{(n-1)} + Q^{(n+1)}$

	this work	Maekawa et al.[10]		
k_n	$CaSiO_3$	Li_2O-SiO_2	Na_2O-SiO_2	K_2O-SiO_2
k_1	0.105 ± 0.019		0.14	0.02
k_2	0.156 ± 0.005	0.30	0.06	0.01
k_3	0.106 ± 0.022	0.08	0.02	0.01

[a] Confidence limits are quoted as ± one unit of standard deviation.

Using our relative $Q^{(n)}$ populations we can calculate for the disproportionation reaction

$$2Q^{(n)} \rightleftharpoons Q^{(n-1)} + Q^{(n+1)} \quad (2)$$

the equilibrium constant at the glass transition temperature,

$$k_n = [Q^{(n+1)}][Q^{(n-1)}]/[Q^{(n)}]^2 \quad (3)$$

For $CaSiO_3$ glass we obtained $k_1 = 0.105 \pm 0.019$, $k_2 = 0.156 \pm 0.005$, and $k_3 = 0.106 \pm 0.022$, respectively. This is the first time equilibrium constants have been measured for alkaline earth silicate glasses. In order to compare with the more studied alkali silicate glasses, we have tabulated equilibrium constant data in Table 3 of alkali silicate data from ref 10. It can been seen that equilibrium constants for calcium silicates are generally larger except in the two cases of k_2 for lithium silicates and k_1 for sodium silicates. Previous work has suggested that more highly charged cations such as Ca^{2+} will shift the disproportionation reaction equilibrium to the right.[6] These results clearly confirm a significant deviation from a binary model[25,26] of $Q^{(n)}$ species disproportionation in alkaline earth silicate melts when compared to alkali silicate melts. While a crystalline composition of $CaSiO_3$ would contain only $Q^{(2)}$ species with alkaline earth cations evenly distributed throughout the lattice, a high equilibrium constant implies an uneven distribution of alkaline earth cations in the glass since the cations would necessarily cluster near the more negative $Q^{(n)}$ species with more nonbridging oxygen (i.e. low n).

As a comparison, we also calculated the disproportionation equilibrium constant k_2 using the fit of the one-dimensional MAS spectrum to three Gaussian line shapes. Results of the fit are also given in Table 2. These values result in a k_2 value of 0.086 ± 0.024, which is significantly lower than those obtained by analyzing the two-dimensional spectrum. Clearly, there is higher uncertainty associated with these results because of the poor resolution in the MAS spectrum compared to the two-dimensional spectrum. Again, the discrepancy in results between the two methods suggested that Gaussian fitting of one-

dimensional MAS spectra is unlikely to be reliable, especially for unresolved spectra, as the case for alkaline earth silicate glasses.

Extensive interpretations of silicate species abundances, and resulting thermodynamics, have been made for Ca-, Sr-, and Ba-silicate glasses and liquids by analyzing Raman spectra.[4,13] Correction factors for Raman band intensities were calibrated using concentrations of $Q^{(1)}$, $Q^{(2)}$, and $Q^{(3)}$ species derived by fitting a published ^{29}Si MAS NMR spectrum of $CaSiO_3$ glass[6] to three Gaussian line shapes. This fit was, unfortunately, not consistent with the glass composition, as the area of the $Q^{(3)}$ peak appears to be considerably larger than that of the $Q^{(1)}$ peak. This NMR spectrum, however, may have been somewhat distorted due to the lower sample spinning speeds available at the time. The $Q^{(3)}$ and $Q^{(1)}$ abundances derived from the calibrated Raman intensities are quite different from those found here, resulting in a k_2 value of 0.032 instead of 0.156. It is clear that the Raman-based models will need to be significantly and systematically adjusted.

Conclusions

We have found that a new two-dimensional NMR approach can give much more robust estimates of silicate species abundances in glasses than can fitting of unresolved peaks in one-dimensional NMR spectra. Using this approach we obtained for the first time the equilibrium constants for the $Q^{(n)}$ disproportionation reaction in $CaSiO_3$. These results confirmed a significantly greater deviation from a binary model of $Q^{(n)}$ disproportionation in alkaline earth silicate melts compared to alkali silicate melts. Results of this kind on a few carefully chosen compositions should lead to a major improvement of structure-based thermodynamic models of silicate liquids.

Acknowledgment. P.J.G. acknowledges support from the National Science Foundation (No. CHE-9501872) and the Donors of The Petroleum Research Fund, administered by the American Chemical Society. J.S. acknowledges support from the National Science Foundation (No. EAR-9506393).

References and Notes

(1) McMillan, P. F.; Wolf, G. H.; Poe, B. T. *Chem. Geol.* **1992**, *96*, 351−366.

(2) McMillan, P. F.; Wolf, G. H. *Vibrational Spectroscopy of Silicate Liquids, Reviews in Mineralogy*; Mineralogical Society of America: Washington, DC, 1995; Vol. 32, Chapter 11, pp 505−562.

(3) Mysen, B. O.; Frantz, J. D. *Contrib. Mineral. Petrol.* **1994**, *117*, 1−14.

(4) Frantz, J. D.; Mysen, B. O. *Chem. Geol.* **1995**, *121*, 155−176.

(5) Mysen, B. O.; Frantz, J. D. *Chem. Geol.* **1992**, *96*, 321−332.

(6) Murdoch, J. B.; Stebbins, J. F.; Carmichael, I. S. E. *Am. Mineral.* **1985**, *70*, 332−343.

(7) Schneider, E.; Stebbins, J. F.; Pines, A. *J. Non-Cryst. Solids* **1987**, *89*, 371−383.

(8) Dupree, R.; Holland, D.; McMillan, P. W.; Pettifer, R. F. *J. Non-Cryst. Solids* **1984**, *68*, 399.

(9) Stebbins, J. F. *Nature* **1987**, *330*, 465.

(10) Maekawa, H.; Maekawa, T.; Kawamura, K.; Yokokawa, T. *J. Non-Cryst. Solids* **1991**, *127*, 53−64.

(11) Libourel, G.; Gieger, C. A.; Merwin, L.; Sebald, A. *Chem. Geol.* **1992**, *96*, 387−397.

(12) Eckert, H. *Prog. NMR Spectroscopy* **1992**, *24*, 159.

(13) Mysen, B. O. *Eur. J. Mineral.* **1995**, *7*, 745−766.

(14) Zhang, P.; Dunlap, C.; Florian, P.; Grandinetti, P. J.; Farnan, I.; Stebbins, J. F. *J. Non.-Cryst. Solids* **1996**, *204*, 294−300.

(15) Smith, K. A.; Kirkpatrick, R. J.; Oldfield, E.; Henderson, D. M. *Am. Mineral.* **1983**, *68*, 1206−1215.

(16) Stebbins, J. F. *Handbook of Physical Constants*; American Geophysical Union: Washington, DC, 1994.

(17) Fyfe, C. A. *Solid-State NMR for Chemists*; (C.F.C. Press: Guelph, 1983.

(18) Engelhardt,G.; Michel, D. *High-Resolution Solid-State NMR of Silicates and Zeolites;* John Wiley & Sons: Chichester, 1987.

(19) Bax, A.; Szeverenyi, N. M.; Maciel, G. E. *J. Magn. Reson.* **1983**, *55*, 494.

(20) Mehring, M. *High Resolution NMR Spectroscopy in Solids, NMR−Basic Principles and Progress*, 2nd ed.; Springer-Verlag: Berlin, 1983; Vol. 11.

(21) Grandinetti, P. J.; Baltisberger, J. H.; Llor, A.; Lee, Y. K.; Werner, U.; Eastman, M. A.; Pines, A. *J. Magn. Reson. A* **1993**, *103*, 72.

(22) Gaskell, D. R. *Metall. Trans.* **1977**, *8B*, 131−145.

(23) Hess, P. C. *Geochim. Cosmochim. Acta* **1971**, *35*, 289−306.

(24) Masson, C. R. *J. Am. Ceram. Soc.* **1968**, *51*, 134−143.

(25) Dupree, R.; Ford, N.; Holland, D. *Phys. Chem. Glasses* **1987**, *28*, (2), 78−84.

(26) Mahler, J.; Sebald, A. *Solid-State NMR* **1995**, *5*, 63−78.